

# Accelerating Molecular Docking Calculations Using Graphics Processing Units

Oliver Korb,<sup>\*†‡</sup> Thomas Stützle,<sup>§</sup> and Thomas E. Exner<sup>\*‡</sup>

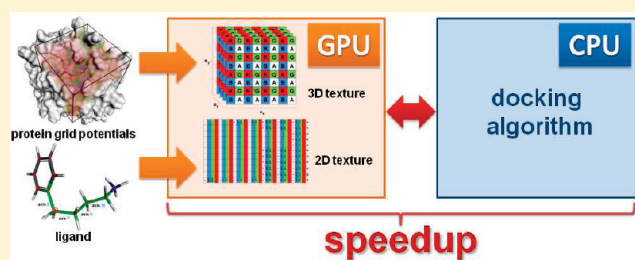
<sup>†</sup>Cambridge Crystallographic Data Centre, CB2 1EZ Cambridge, United Kingdom

<sup>‡</sup>Department of Chemistry and Zukunftskolleg, University of Konstanz, D-78457 Konstanz, Germany

<sup>§</sup>IRIDIA, CoDE, Université Libre de Bruxelles (ULB), Brussels, Belgium

 Supporting Information

**ABSTRACT:** The generation of molecular conformations and the evaluation of interaction potentials are common tasks in molecular modeling applications, particularly in protein–ligand or protein–protein docking programs. In this work, we present a GPU-accelerated approach capable of speeding up these tasks considerably. For the evaluation of interaction potentials in the context of rigid protein–protein docking, the GPU-accelerated approach reached speedup factors of up to over 50 compared to an optimized CPU-based implementation. Treating the ligand and donor groups in the protein binding site as flexible, speedup factors of up to 16 can be observed in the evaluation of protein–ligand interaction potentials. Additionally, we introduce a parallel version of our protein–ligand docking algorithm PLANTS that can take advantage of this GPU-accelerated scoring function evaluation. We compared the GPU-accelerated parallel version to the same algorithm running on the CPU and also to the highly optimized sequential CPU-based version. In terms of dependence of the ligand size and the number of rotatable bonds, speedup factors of up to 10 and 7, respectively, can be observed. Finally, a fitness landscape analysis in the context of rigid protein–protein docking was performed. Using a systematic grid-based search methodology, the GPU-accelerated version outperformed the CPU-based version with speedup factors of up to 60.



## INTRODUCTION

The most time-consuming step in most docking programs,<sup>1</sup> the evaluation of the scoring function, is usually carried out on the central processing unit (CPU). This also applies to our protein–ligand docking approach PLANTS, which is described in detail elsewhere.<sup>2–4</sup> Here, a novel approach is presented that is capable of exploiting the computational power available on today's graphics processing units (GPUs) for accelerating this step considerably. During the past several years, GPUs have become an alternative to purely CPU-based high-performance computing.<sup>5</sup> This can be attributed, on one hand, to the moderate costs of only a few hundred dollars/euros for a consumer graphics card and, on the other hand, to the enormous floating-point performance offered for scientific calculations. According to Owens et al.,<sup>6</sup> the performance of GPUs increases with a yearly rate of 1.7 (pixels per second) to 2.3 (vertices per second), on average, much faster than the performance of CPUs, which exhibited an average increase of 1.4. A large fraction of the performance increase observed for new GPU generations can be attributed to the addition of extra stream processors. The development of the floating-point performance measured over the past several years for CPUs and GPUs is presented in Figure 1. For example, the Nvidia GeForce 8800 GTX GPU used in this work offers 128 stream processors and is theoretically capable of performing up to 500 GFLOPS

(Giga-FLOPS, billion floating-point operations per second, single precision). Note that the performance observed in practice depends strongly on the algorithm and the problem instance used. Whereas former-generation GPU hardware was developed exclusively for visualization and thus offered only a fixed function pipeline, current-generation GPUs can be programmed with CPU-like programming languages and offer much more flexibility.

In the following discussion, a general outline for speeding up the scoring function evaluation process is explained, which can, in principle, be applied to any existing docking approach. Additionally, preliminary results are presented for a modified parallel version of PLANTS that makes use of the GPU-accelerated scoring function evaluation step. It must be noted that the present approach is based on the old graphics pipeline methodology, whereas special toolkits for general-purpose computation on GPUs are available today (e.g., compute unified device architecture, CUDA<sup>7</sup>), which avoid some of the overheads associated with calculations using the graphics pipeline. A reimplementation of the GPU-based scoring function evaluation presented herein using these toolkits could lead to a further increase in performance. Nevertheless, the parallel decomposition schemes used here are

Received: November 24, 2010

Published: March 24, 2011

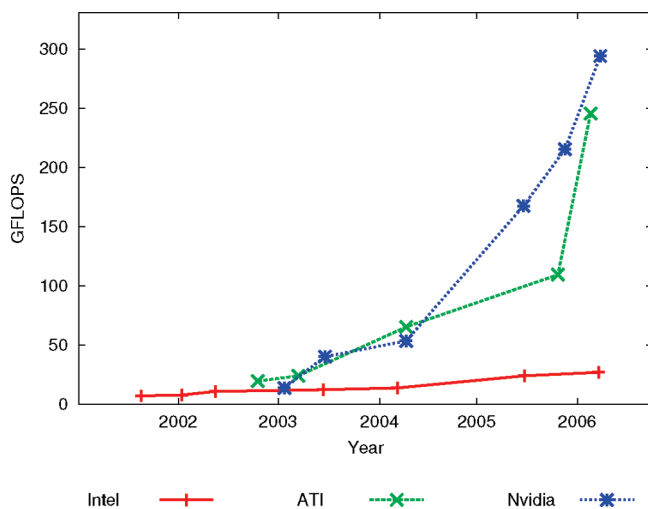


**Figure 1.** Development of the floating-point performance for CPUs (Intel) and GPUs (AMD/ATI, Nvidia) over the past several years measured on the multiply-add instruction (MAD), counting two floating-point operations per MAD, according to Owens et al.<sup>6</sup>

generally applicable and independent of the actual implementation (see also ref 8).

Several fields of research already profit from using GPUs for computational tasks, ranging from standard algorithms such as sorting, searching, and reduction to physically based simulation. The reported speedup factors compared to the respective purely CPU-based implementations are in the range of nearly no improvement to speedup factors of over 100, clearly dependent on the problem domain. For an extensive overview, we refer to Owens et al.<sup>6</sup> and references therein. In the field of computational chemistry, especially quantum mechanical calculations<sup>9–12</sup> and molecular dynamics simulations<sup>13–15</sup> have benefited from GPU acceleration. A review of these and other computational chemistry applications was published recently by Stone et al.<sup>8</sup> In contrast, the possibilities for molecular docking have been exploited only to a limited degree. The evaluation of molecular interaction potentials was described by Roh et al.,<sup>16</sup> and a rigid protein–ligand docking program was presented by Sukhwani et al.<sup>17</sup> For several reasons, these approaches are not directly comparable to the work presented here. First, our method treats the ligand conformation and also donor groups in the protein structure as flexible, whereas the other approaches use rigid molecules. Second, our primary test set, a subset of the well-known CCDC/Astex clean list,<sup>18</sup> is composed of pharmaceutically relevant protein–ligand complexes. It consists of 129 protein–ligand complexes containing small to medium-sized ligands reflecting the composition of real-world virtual screening databases. Given that there is a correlation between the speedup factors and the problem instance size because of a higher arithmetic intensity for larger problem instances, it will be harder to obtain reasonable speedup factors for these small ligands compared to protein–protein complexes or very large ligands. Usually, high speedup factors are observed for large instances, but no or only minor speedup factors are observed for small ones. Thus, the speedup reported for a study crucially depends on the composition of the test set. That this is also the case for our approach will be shown for the protein–ligand test set but also for a small set of protein–protein complexes.

For a comparison, the algorithmic complexity of the approaches also has to be taken into account. The worst-time complexity of the

energy evaluation step in the study of Roh et al.<sup>16</sup> is  $O(n \times m)$ ; that is, all pairs of  $n$  ligand and  $m$  protein atoms are evaluated. However, when the protein structure is kept rigid, there are efficient ways to evaluate the protein–ligand potentials in linear time,  $O(n)$ . In many molecular modeling applications, a distance cutoff is introduced for the potential function, for example, 8–12 Å for Lennard-Jones potentials or 5.5 Å for the piecewise linear potential.<sup>19</sup> In this case, spatial data structures such as regular grids can be used to reduce the complexity to  $O(k \times n)$ , where  $k$  is the number of protein atoms within the cutoff distance. Because  $k$  has an upper bound that is independent of the number of protein atoms  $m$  (i.e., there is a limit on the number of atoms that fit into the cutoff distance),  $O(k \times n)$  reduces to  $O(n)$ . This approach for the evaluation of the potential function is exact (with respect to the cutoff). If no gradient information is needed, another  $O(n)$  approach can be used, which can also be applied if the potential function has no cutoff distance. For each ligand atom type, the potential function contributions are precomputed on a separate grid. At evaluation time, for each ligand atom, the potential value is looked up in the appropriate grid by either a nearest-neighbor or trilinear interpolation approach, and all individual contributions are accumulated. Although this evaluation method is not exact, it is used in almost all docking programs, including ours, because of its speed. The docking accuracies achieved by the different evaluation approaches are still comparable. Note that the arithmetic intensity (i.e., the number of floating-point operations carried out) of the  $O(n \times m)$  approach is much higher than that of the  $O(n)$  approach used in this work, and thus, comparing a GPU-based and CPU-based implementation of an  $O(n \times m)$  approach will result in much higher speedup factors. However, the absolute run time of the linear-time interpolation [ $O(n)$ ] approach is, on average, much shorter than summing over all protein–ligand atom pairs [ $O(n \times m)$ ].

In this work, we try to address many of the issues mentioned. We present GPU-accelerated versions of two scoring functions using the efficient evaluation approaches presented above and also introduce a novel parallel version of PLANTS using multiple ant colonies. A GPU-accelerated version of the parallel PLANTS algorithm is compared not only with the same algorithm running on the CPU, but also with the optimized CPU-based sequential PLANTS algorithm. We made this last comparison specifically because we believe that a GPU-accelerated docking approach should not only be considerably faster than the CPU-based version, but, more importantly, still deliver the same pose prediction performance comparable to state-of-the-art docking programs when assessed on large data sets.

## MATERIALS AND METHODS

**GPU Implementation.** In the following section, we describe the encoding of the protein and ligand data in more detail. The implementation was carried out using OpenGL to access the GPU's graphics pipeline and Nvidia's Cg language for implementing the specific fragment shader programs (i.e., the algorithms performing the actual calculations on the GPU). Although our approach is unique and efficient with respect to the way it exploits certain features of the graphics pipeline, it is important to remark that the parallel decomposition schemes used to speed up the structure transformation and scoring function evaluation steps are general and can, in principle, be implemented using any GPU library designed for parallel computation, such as CUDA or OpenCL (Open Computing Language<sup>20</sup>).

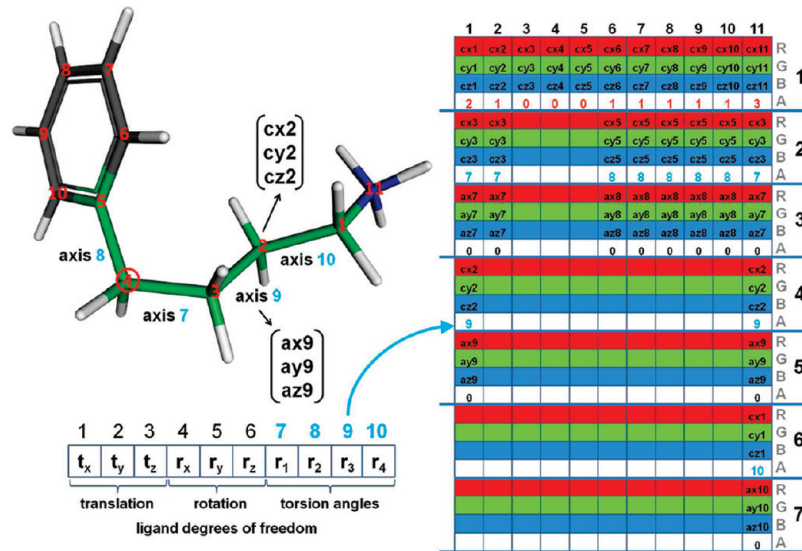


**Figure 2.** Illustration of the ligand transformation process exemplified for 4-phenylbutylamine (PDB code 1tni). Each column in the RGBA texture shown to the right encodes the operations needed to transform one ligand atom. For example, column 1 describes which rotatable bonds and atoms are involved in transforming atom 1. Atom number 4 (marked with a red circle) is the root of the two kinematic chains (first one along axis 8; second one along axes 7, 9, and 10) and also the origin for the local coordinate system used to define the rigid-body degrees of freedom. The RGB channels of the first row represent the coordinates of the atom to be transformed. The alpha channel (A) defines the number of rotatable bonds involved in the transformation of the respective atom, for example, 2 in the case of atom 1. The first row is followed by pairs of representative coordinates for a rigid fragment and the corresponding rotatable-bond vectors. For example, the RGB channels of the second row in the first column represent the coordinates of atom 3 as representative of the fragment transformed by the rotatable bond vector of axis 7 specified in the third row. The alpha channel of the second row points to the corresponding degree of freedom in the ligand transformation texture, which specifies the torsion angle selected for this rotatable bond. The values for the translational, rotational, and torsional degrees of freedom determining the final ligand conformation are specified in a separate texture.

All data need to be encoded into textures to be available for GPU-based calculations. Because many ligands are docked to the same protein structure in virtual screening applications, the protein data structures are set up only once in the preprocessing stage. This primarily involves atom-typing, detection of rotatable donor groups within the predefined binding site, and precalculation of the scoring function grids used later on for the scoring of protein–ligand interactions. Similar steps are carried out for each ligand to be docked. The required time for ligand preparation is negligible compared to that required for the protein setup, so that here no advantage can be gained by GPU acceleration. In addition to these tasks also performed in the CPU version, all of these data need to be encoded appropriately to be processed by the GPU. In the second stage, at run time, the preprocessed data are used for performing the structure transformations and scoring function evaluations on the GPU.

**Scoring Function Modifications.** For both empirical scoring functions available in PLANTS, PLANTS<sub>plp</sub> and PLANTS<sub>chemplp</sub>, a GPU-accelerated version has been implemented. For the form and parametrization of the scoring functions, we refer to our previous work.<sup>4</sup> Whereas the implementation of scoring function PLANTS<sub>plp</sub> was straightforward, some parts of the scoring function PLANTS<sub>chemplp</sub> had to be modified. Some of the spatial data structures used in the CPU implementation could not directly be mapped to the GPU programming model because of missing support for shared memory operations on older-generation hardware, which was used for the development. Thus, the GPU-accelerated version of PLANTS<sub>chemplp</sub> at the moment lacks support for angle-dependent scoring of bonding to metal ions in the protein binding site, as well as for CH–O hydrogen bonding. Additionally, the standard version<sup>4</sup> of PLANTS<sub>chemplp</sub> limits all protein and ligand

donor hydrogens to form at most one hydrogen bond. In the GPU-based implementation, this condition was applied only for the ligand. To approximately achieve the same behavior for both versions, all ligand acceptor atoms were restricted to form at most as many hydrogen bonds as lone pairs were available. Note that we implemented the same changes for PLANTS<sub>chemplp</sub> in the CPU-based version to allow for a direct comparison of the two approaches. Thus, all results presented in this work refer to the modified versions of PLANTS<sub>chemplp</sub>.

**Preprocessing.** During the preprocessing stage, static data that only need to be prepared once are transferred to the GPU. To allow for a parallel transformation of the ligand atoms as well as the rotatable donor groups of the protein at run time, the kinematic chain for each atom is encoded into a two-dimensional texture starting from the root atom to the atom to be transformed. This encoding scheme, as used in the shader program on the GPU later on, is illustrated for ligand structure 4-phenylbutylamine [Protein Data Bank<sup>21</sup> (PDB) code 1tni] in Figure 2 when using scoring function PLANTS<sub>plp</sub> (neglects all hydrogen atoms). Each column of the RGBA texture encodes the operations needed to calculate the transformed coordinates of one atom in the molecule. Because of the atom-wise treatment of the molecular transformation step, all atoms can be transformed concurrently on several stream processors at a time. For the ligand, additional textures storing the information for the clash potential and the torsional potential for each rotatable bond are transferred to the GPU.

The piecewise linear potential (PLP) is precalculated on the CPU for all four ligand atom types (donor, acceptor, donor/acceptor, nonpolar) and stored in separate grids (see Figure 3). This representation fits perfectly to a special kind of texture

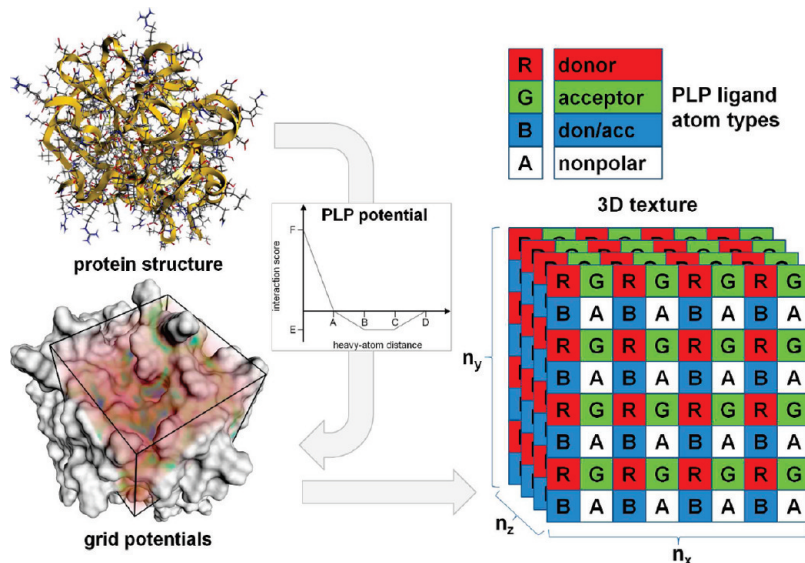


**Figure 3.** Illustration of the preprocessing stage. The PLP interaction potentials are precalculated on the CPU and stored on the GPU in a three-dimensional RGBA texture of size  $n_x \times n_y \times n_z$  covering the protein binding site. The potentials for the four different ligand atom types are stored in the red, green, blue, and alpha channels of the three-dimensional texture.

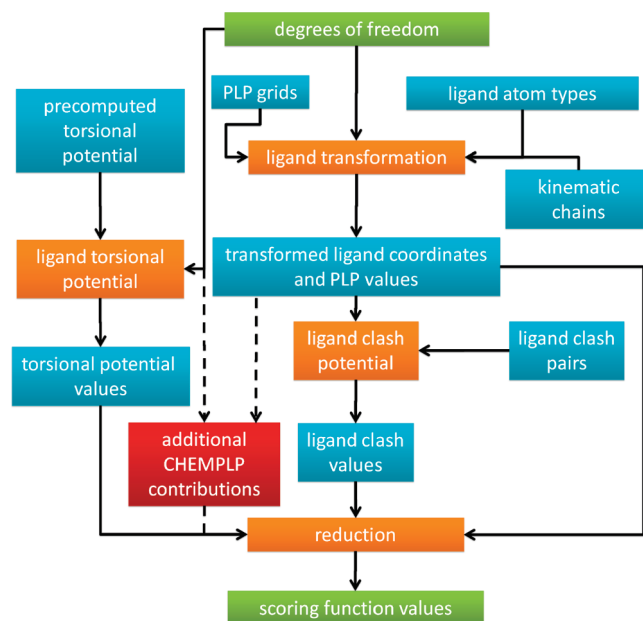


**Figure 4.** Illustration of the GPU-based scoring function evaluation step for scoring function  $\text{PLANTS}_{\text{plp}}$  (additional contributions are calculated for scoring function  $\text{PLANTS}_{\text{chemplp}}$ ). Green boxes represent textures involved in CPU/GPU data transfers. Blue boxes are textures transferred once to GPU memory and used for calculations, whereas shader programs performing the actual calculations are shown in orange. First, the values for all degrees of freedom are transferred to the GPU ( $p$  ligand conformations in parallel). Then, a multipass rendering algorithm draws several rectangles, thereby invoking the execution of the shader programs. In the first step, the ligand atoms are transformed, and the resulting data are used to calculate all scoring function contributions in subsequent rendering passes. These contributions are finally accumulated to  $p$  scoring function values (reduction), which are transferred back to the CPU.

available on GPUs, called three-dimensional or volume textures. A single 16-bit floating-point RGBA three-dimensional texture is

created residing in the GPU's onboard memory, and the four grids are transferred from the CPU and stored in the red, green, blue, and alpha channels of this texture. This enables the approach to profit from the GPU's hardware-accelerated trilinear interpolation capabilities. In the case that a scoring function uses more than four ligand atom types, the approach can be easily extended to use multiple textures.

If scoring function  $\text{PLANTS}_{\text{chemplp}}$  is used, additional textures storing information about donor and acceptor groups in the protein binding site and the ligand are encoded. In this case, kinematic chains for all rotatable donor groups in the protein binding site are also stored in a texture similar to the encoding presented for the ligand (see Figure 2).

**Run Time.** At run time, the multipass rendering algorithm illustrated in Figure 4 is executed. Although only a short summary of the steps is given here, a more detailed description of the texture encoding used can be found in Figures S1–S4 of the Supporting Information. In total,  $n \times p$  floating-point values are transferred to the GPU, where  $n$  is the problem dimension (i.e., the number of ligand and protein degrees of freedom) and  $p$  is the number of conformations that are transformed and scored in parallel.

**Ligand Transformation and PLP Scoring.** In the first rendering pass, the ligand transformation shader takes the textures encoding the ligand representation (Figure 2), the precalculated PLP grids (Figure 3), the degrees of freedom (Figure S2a, Supporting Information), and the ligand atom types as input (Figure S2b, Supporting Information). All atoms are transformed, and the resulting coordinates are used to fetch the appropriate PLP potential value from the three-dimensional texture. Coordinates and potential values are stored in an RGBA texture depicted in Figure S1 (Supporting Information).

**Ligand Clash Potential.** For the ligand clash potential calculation, the precomputed ligand coordinates (Figure S1, Supporting Information) and a texture encoding the clash pairs to be evaluated are used (Figure S3, Supporting Information). The shader evaluates four clash pairs at the same time in order to increase the arithmetic intensity. The texture storing the clash

pairs to be evaluated is thus extended by dummy pairs if the total number of pairs is not a multiple of four.

**Ligand Torsional Potential.** The torsional potential shader takes as input the degrees of freedom texture and the texture in which the precomputed torsion values to a resolution of  $0.1^\circ$  are stored. For each rotatable bond, the appropriate potential value is then looked up (see Figure S4, Supporting Information).

**ChemPLP.** If scoring function PLANTS<sub>chemplp</sub> is used, additional shaders are executed to perform the scoring of distance- and angle-dependent hydrogen bonds. In that case, rotatable donor groups in the protein binding site are also transformed.

**Reduction.** In the last step, all of the calculated data for each of the  $p$  conformations are reduced to a single scoring function value by accumulating the partial results. These  $p$  score values are transferred back to the CPU (see Figure S2a, Supporting Information).

**PLANTS<sup>GPU</sup>.** The PLANTS algorithm<sup>2–4</sup> was initially designed for sequential execution on the central processing unit (CPU). The most efficient search parameter settings identified for this version<sup>4</sup> all use 20 ants for the artificial ant colony, which turned out to result in a good optimization performance. However, as will be shown later, at least  $p = 100$  conformations must be scored in parallel in the GPU-accelerated framework to reach a speedup over the purely CPU-based version. Therefore, a parallel version of the PLANTS algorithm that exploits the parallel nature of the GPU-accelerated scoring function evaluation step is introduced here.

**Parallel PLANTS.** Parallel versions of ant colony optimization (ACO) algorithms have already been proposed in the literature. Essentially, two main research directions have been followed: The first is to speed up a single run of an ACO algorithm through parallelization,<sup>22,23</sup> whereas the second is to use multiple ant colonies in parallel and to occasionally exchange information between them.<sup>24,25</sup> In the latter case, the goal often is to design effective communication strategies to increase the solution quality obtained. A noteworthy exception to these directions is the specific design of an ACO algorithm to allow an effective hardware implementation on field-programmable gate arrays (FPGAs).<sup>26</sup>

We follow the second direction. Thus, multiple ant colonies are employed in parallel. For the parallel version, we also removed the refinement local search from the sequential PLANTS algorithm, because the refinement local search is a purely sequential step and hinders an effective implementation (see ref 3 for details on the usage of the refinement local search). Additionally, the Nelder–Mead simplex algorithm<sup>27</sup> has been modified to locally minimize  $p$  solutions in parallel. In addition to a maximum number of 5000 objective function evaluations and a termination criterion taking the fractional range of the best and worst solutions in the simplex into account,<sup>28</sup> another termination criterion has been added to avoid unnecessary long simplex descents. In particular, a simplex run is terminated if more than  $1.5n_b$  iterations have been carried out, where  $n_b$  is the number of simplex iterations carried out by the best-performing simplex run (best of  $p$  simplex runs in each iteration) in the last ACO iteration. In the first iteration,  $n_b$  is set to 2000 iterations. Without this additional termination criterion, each of the  $p$  optimization runs would terminate after a different number of iterations. Thus, in the worst case,  $p - 1$  optimization runs have already terminated after, say, 100 iterations, whereas one run needs, say, 1000 iterations. To compensate for the missing refinement

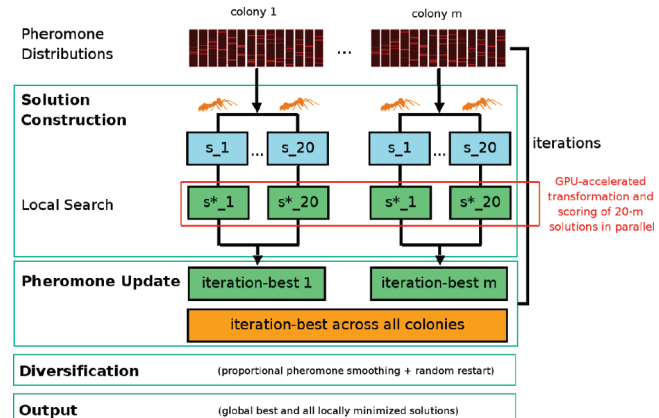


**Figure 5.** Flowchart for the GPU-accelerated version of PLANTS. In contrast to the sequential algorithm,  $m$  artificial ant colonies are used, allowing for the transformation and scoring of  $20m$  solutions in parallel on the GPU. All other steps of the algorithm are carried out on the CPU.

local search, the parameter for the simplex tolerance termination criterion was set to  $\text{nms}_{\text{tol}} = 0.0075$ , which is a smaller value than the default value in the sequential PLANTS algorithm. These modifications were necessary to allow for an efficient parallel execution of the scoring function evaluation step for all artificial ants across all colonies used.

An algorithmic outline of the parallel PLANTS implementation can be found in Algorithm 1 as well as in Figure 5. For each colony, it follows the general ACO scheme regarding the step solution construction and pheromone update. Additionally, in the middle part, the above-described version of the Nelder–Mead simplex algorithm is employed to perform a local optimization of all solutions generated by the probabilistic construction step of the ACO algorithm. The values of the degrees of freedom obtained for the best solution identified in any of these local optimization runs are then used for updating the pheromone distribution. In a PLANTS iteration, the solution construction, the generation of new simplices for the local optimization, and the pheromone update are carried out on the CPU; the structure transformation and scoring function evaluation are performed entirely on the GPU (in procedure ParallelLocalSearch<sup>GPU</sup>). During the pheromone update phase, the iteration-best ant  $s_j^{\text{ib}}$  of each colony  $j$  is allowed to deposit pheromones. Additionally, for all  $f_{\text{update}}$  iterations, the iteration-best ant across all colonies deposits a pheromone intensity of  $0.5f(s^{\text{ib}})$  on each colony's pheromone values. The search diversification criteria are the same as for the sequential algorithm. The ACO algorithm is run for a specified number of iterations

$$\max_{\text{iterations}} = \sigma \frac{10}{\text{colonies} \times \text{ants}} (100 + 50 \times \text{lrb} + 5 \times \text{lha}) \quad (1)$$

where lrb is the number of rotatable bonds, lha is the number of heavy atoms in the ligand, and  $\sigma$  is a factor scaling the number of ACO iterations. We set the number of ants for each colony to 20 for all experiments. When the algorithm terminates, the same clustering algorithm as described for the sequential version<sup>3</sup> is executed for the set  $M$  containing all locally minimized solutions. In addition to the global best solution,  $s^{\text{gb}}$ , a set of geometrically diverse solutions is returned.

Algorithm 1 PLANTS<sup>parallel</sup>

```

InitializeParametersAndPheromones()
M ← 0
for i = 1 to max_iterations do
    S ← 0
    for j = 1 to number_of_colonies do
        for k = 1 to number_of_ants do
             $s_{jk} \leftarrow \text{ConstructSolution}()$ 
            S ← S ∪  $s_{jk}$ 
        end for
    end for
     $S^* \leftarrow \text{ParallelLocalSearch}^{\text{GPU}}(S)$ 
     $s^{\text{ib}} \leftarrow \text{GetIterationBestSolution}(S^*)$ 
    M ← M ∪  $S^*$ 
    for j = 1 to number_of_colonies do
         $s_j^{\text{ib}} \leftarrow \text{GetIterationBestSolutionOfColony}()$ 
        UpdatePheromones( $s_j^{\text{ib}}$ )
        if(cross-colony update criteria met) then
            UpdatePheromones( $s^{\text{ib}}$ )
        end if
        if (diversification criteria met) then
            ApplySearchDiversification()
        end if
    end for
end for
 $s^{\text{gb}} \leftarrow \text{GetGlobalBestSolution}(M)$ 
return M,  $s^{\text{gb}}$ 

```

To identify reasonable settings for the evaporation factor  $\rho$  and the number of iterations after which the iteration-best solution across all colonies is allowed to update all other colonies, the update frequency,  $f_{\text{update}}$ , a parameter optimization using six protein–ligand complexes (PDB codes 1a4g, 1fax, 1ppc, 1rob, 1tyl, and 4dfr) was carried out. For parameter,  $\rho$  the values 0.5, 0.6, 0.7, 0.8, and 0.9 were tested, whereas for  $f_{\text{update}}$  values of 2 and 4 were considered. Finally, for  $\sigma$  values of 0.5, 0.75, 1.0, 1.25, 1.5, and 1.75 (scoring function PLANTS<sub>plp</sub> only) were tested. All results were averaged over 40 independent runs.

**Fitness Landscape Analysis.** To exploit the full potential of the approach presented in this work, we also performed a fitness landscape analysis in the context of rigid protein–protein docking. This kind of analysis gives insight into the distribution of local optima and can thus be useful for scoring function or search algorithm design. For each protein–protein complex, the translational and rotational degrees of freedom of one protein were sampled using a grid-based approach. To sample the translational degrees of freedom, a uniform grid was placed in the a priori defined binding site, and the center of the mobile protein’s coordinate system was placed onto each grid point. For each placement, 4000 uniformly distributed rotations were generated, and the best resulting scoring function value (scoring function PLANTS<sub>plp</sub>) was recorded. In the GPU-accelerated version, these 4000 conformations were scored in parallel. Additionally, for each grid point, the heavy-atom rmsd (root-mean-square deviation) of the best conformation was calculated with respect to the experimentally observed conformation. The size of the uniform grid was chosen to enclose the conformation of the mobile protein as observed in the experimentally determined protein–protein complex. Finally, to identify the global optimum, the structures with scores below –50.0 au

identified by the systematic search were further optimized by the rigid-body local minimization based on the Nelder–Mead simplex algorithm<sup>27</sup> implemented in PLANTS.

## ■ RESULTS AND DISCUSSION

**Assessment of Accuracy and Performance.** Because of the scoring function adaptations needed for the GPU implementation, in a first step, the accuracy of the GPU-accelerated version was assessed by calculating the deviation  $|f_{\text{CPU}} - f_{\text{GPU}}|$  of the scoring function values  $f_{\text{CPU}}$  and  $f_{\text{GPU}}$  as obtained from the CPU- and GPU-based evaluations, respectively. For these experiments, 17 protein–ligand complexes from the CCDC/Astex data set<sup>18</sup> of different sizes with ligands containing between 0 (PDB code 1acj) and 28 (PDB code 1ppi) rotatable bonds were selected (number of rotatable bonds according to scoring function PLANTS<sub>chemplp</sub>, which also considers rotatable donor groups such as  $-\text{OH}$  and  $-\text{NH}_3^+$ ). In the context of rigid protein–protein docking, similar experiments were carried out for 18 protein–protein complexes (PDB codes and compound names are given in Table S1 in the Supporting Information). For these complexes, the number of heavy atoms of the mobile protein ranged from 157 (PDB code 2cpk) to 1001 (PDB code 3hfm). In 17 of the 18 complexes, the mobile protein is a peptidic inhibitor, in most cases in complex with a protease. The other example is lysozyme bound to the FAB antibody fragment (PDB code 3hfm). All structures were taken from the Protein Data Bank.<sup>21</sup> Hydrogens and missing heavy atoms were added and optimized using the AMBER 10 program package.<sup>29</sup> For each protein–protein complex, the binding site was defined by a box enclosing the experimentally determined structure of the mobile protein, extended by 10 Å in each direction. The resulting binding site volumes ranged from  $62.76^3 \text{ \AA}^3$  for PDB code 2cpk to  $75.64^3 \text{ \AA}^3$  for PDB code 3hfm.

For each complex, 5 million random conformations were generated and scored. Although the average deviation of the scoring function values for the protein–ligand complexes studied was between 0.03 and 0.08 scoring function units, the maximum deviations observed could be as large as 1.3 scoring function units depending on the ligand. Because of the larger size of the molecules in the protein–protein data set, the average deviations range from 0.13 (PDB code 2cpk) to 0.30 (PDB code 3hfm). All results are reported in Tables S2–S4 in the Supporting Information. Further investigations revealed that these deviations can be exclusively attributed to the differences in the trilinear interpolation of the PLP scoring function grids. In our GPU implementation, these grids were stored in an RGBA 16-bit floating-point format in GPU memory, and hence, the trilinear interpolation operation executed to calculate the PLP scoring function value for each ligand heavy atom is also carried out in 16-bit precision only. In contrast, a 32-bit trilinear interpolation was used in the CPU-based version. The average accuracy of the GPU approach is still precise enough to be used in molecular docking calculations. However, when performing a virtual screening experiment with the CPU- and GPU-based versions, slightly different rankings could be obtained for ligands with similar scoring function values.

In a second step, the performance of each implementation with respect to the time needed to perform 3 million scoring function evaluations was assessed. For the structure transformation and scoring function evaluation, the relative performances of a Nvidia GeForce 8800 GTX based GPU and a single core of a

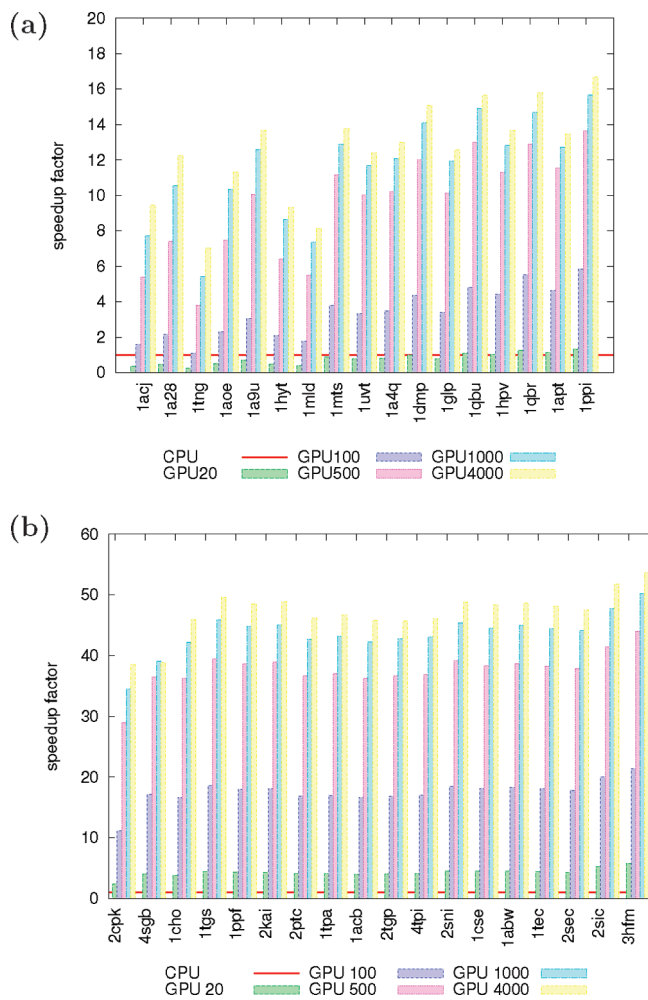


**Figure 6.** Comparison of CPU- and GPU-based structure transformation and scoring function evaluation. The scoring function was evaluated 3 million times on a Pentium 4, 3.0 GHz CPU and a Nvidia GeForce 8800 GTX GPU for different numbers of conformations in parallel (GPU  $x$  means that  $x$  conformations are evaluated in parallel). The speedup factor is calculated by dividing the time measured for the CPU-based approach by the time measured for the GPU. Thus, the speedup factor of the CPU-based approach (shown as a red line) is 1. In general, a higher speedup factor is better. The results include data transfer times to the GPU and back. Results are presented for (a) protein–ligand complexes (flexible ligand) and (b) protein–protein complexes (rigid mobile protein) when using scoring function PLANTS<sub>plp</sub>.

Dual Core Pentium 4, 3.0 GHz CPU were calculated [i.e., the time measured for the CPU divided by the time needed by the GPU for the same number of evaluations (these two architectures represented the state-of the-art when the project was started)]. Results for the performance evaluation when using scoring function PLANTS<sub>plp</sub> for protein–ligand and protein–protein complexes can be found in parts a and b, respectively, of Figure 6. Results for scoring function PLANTS<sub>chemplp</sub> can be found in Figure S5 in the Supporting Information. For protein–ligand complexes, PDB codes are sorted according to increasing numbers of rotatable bonds from left to right, whereas for protein–protein complexes, the number of heavy atoms in the mobile protein was used. For the GPU, different numbers of structures scored in parallel were investigated (20, 100, 500, 1000,

and 4000). Because of the problem encoding scheme used, the maximum number of structures that could be scored in parallel was limited by the texture dimension limit of 4096 pixels on older-generation hardware (Nvidia GeForce 6 and 7 series GPUs were used for the development). For protein–ligand complexes, it can be seen in Figure 6a that the CPU implementation was clearly outperformed, with speedup factors of up to 16 (PDB code 1ppi, 4000 scoring function evaluations in parallel), which is a very encouraging result. However, from the chart, it is obvious that at least 100 conformations must be evaluated in parallel to reach a speedup over the CPU implementation. This can be explained by the fact that the arithmetic intensity (i.e., the number of actually performed floating-point operations) on the GPU is too low in the case of, for example, only 20 conformations, because much time is spent for the data transfer from the CPU to the GPU and especially back (depending on the computer architecture used). Whereas for the 3 million scoring function evaluations, the data transfer is invoked 150000 times when evaluating 20 conformations in parallel, it is invoked only 30000 times when evaluating 100 conformations in parallel. As expected, the speedup factors observed for protein–protein complexes (Figure 6b) are much higher than those for protein–ligand systems. When scoring 4000 protein complexes in parallel, speedup factors from around 40 up to over 50 can be observed depending on the protein–protein complex. From Figure 1b, it is also obvious that already 20 protein structures scored in parallel are sufficient to gain a speedup over the CPU-based implementation in this case.

The actual speedup observed for all investigated complexes is dependent on the complexity of the ligand (protein) and on the number of structures scored in parallel. The approach generally profits from ligands with many rotatable bonds, a large number of heavy atoms, and larger numbers of parallel evaluations. In these cases, the arithmetic intensity is much higher, which allows for an efficient utilization of all stream processors available on the GPU. Even if these results suggest that as many parallel structures as possible should be used, for the performance of the docking algorithm, additional considerations have to be taken into account. On one hand, using the modified parallel version of PLANTS, more structures can be transformed and scored in parallel when the number of artificial ant colonies is increased. On the other hand, a single ACO run has fewer iterations available to learn a good solution if the same number of scoring function evaluations are performed (see eq 1). As a compromise, we set the number of artificial ant colonies to either 20 or 25, resulting in 400 or 500 parallel scoring function evaluations, respectively. According to the performance assessment presented above, these settings were expected to result in speedup factors of up to 10 for drug-like ligands with up to 10 rotatable bonds.

**Docking Results.** For the search parameter optimization and the final docking experiments, a restricted list of complexes from the CCDC/Astex data set<sup>18</sup> was used as the primary test set. From the 213 complexes of the clean list<sup>ac</sup> (noncovalently bound complexes), 40 structures containing metal ions in the binding site were removed. Additionally, only drug-like ligands with up to 10 rotatable bonds were considered, resulting in 135 unique protein–ligand complexes. From this set, the 6 complexes used for the search parameter optimization procedure described above were also removed to get the final independent test set of 129 complexes for the assessment of pose prediction accuracy. All experiments were carried out on a single core of a Pentium 4, 3.0 GHz processor. The GPU-accelerated approach used the same test

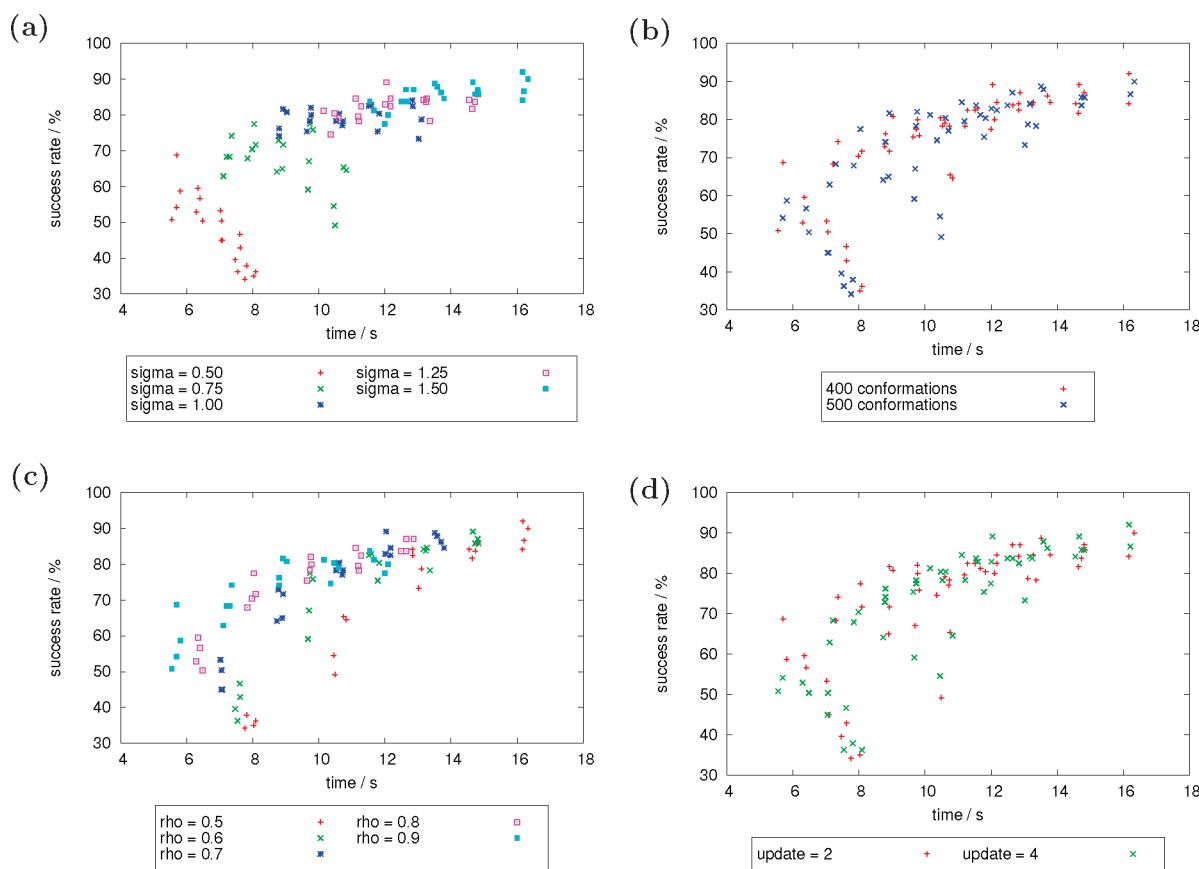


**Figure 7.** Influence of different settings for (a) parameter  $\sigma$  scaling the number of ACO iterations, (b) the number of conformations scored in parallel, (c) the evaporation factor  $\rho$  and (d) the cross-colony solution update frequency  $f_{\text{update}}$  on the optimization performance when using scoring function PLANTS<sub>chemplp</sub>. In each graph, the average docking time per ligand is reported on the  $x$  axis, while the  $y$  axis shows the success rate reached. A success was obtained if the top-ranked solution had a rmsd lower than 2 Å compared to the experimentally determined structure. All results are averaged over 40 runs.

system as for the CPU-based calculations (i.e., all calculations concerning the ACO and simplex local search algorithm), whereas the GPU-based structure transformation and scoring function evaluation were carried out on a Nvidia GeForce 8800 GTX GPU. The observed times, success rates, and numbers of scoring function evaluations were averaged over 40 independent runs in the search parameter optimization and over 25 independent runs for the final docking experiments. In all experiments, the spherical binding site definitions as given in the CCDC/Astex data set were used. The ligand structures were randomized with respect to their translational, rotational, and torsional degrees of freedom prior to any docking experiment. A success was obtained if the heavy-atom rmsd between the predicted and experimentally determined ligand conformations was less than 2 Å.

**Search Parameter Optimization.** The influence of the different settings for the search algorithm parameters on the optimization performance is shown in Figure 7 for scoring function PLANTS<sub>chemplp</sub>. In Figure 7a, five clusters can be observed, which correspond to the different settings for parameter  $\sigma$  scaling the number of ACO iterations. As expected, with increasing  $\sigma$ , both the average search time per ligand and the average success rate increase. When looking at the number of structures scored in parallel, the settings performing 400 evaluations concurrently seem to result in slightly better optimization performance on average. This is not surprising because, for this setting (20 ants and 20 colonies compared to 20 ants and 25 colonies when

scoring 500 structures in parallel), more ACO iterations are carried out according to eq 1. The trends observed for evaporation factor  $\rho$  (see Figure 7c) also follow our expectations: For very short optimization times, a high evaporation rate is needed to force the ant colonies to converge to a solution within this time, whereas for longer search times, lower evaporation rates become more favorable. Finally, Figure 7d shows the influence of the cross-colony update frequency,  $f_{\text{update}}$ . Again, for short search times (low  $\sigma$  values), fewer ACO iterations are carried out, and thus, a more frequent update, such as every second iteration, is beneficial for the optimization performance. When more ACO iterations are carried out, a less frequent update results in a slightly better optimization performance.

From this analysis, different search parameter settings have been identified for scaling between search time and optimization performance. A similar analysis was carried out for scoring function PLANTS<sub>plp</sub>, and the resulting settings for both scoring functions (called chemplp\_gpu1 to chemplp\_gpu3 and plp\_gpu1 to plp\_gpu3, respectively) are reported in Table S5 in the Supporting Information.

**Pose Prediction.** The optimized search parameter settings were used to dock the 129 protein–ligand complexes described above running the parallel PLANTS algorithm on the CPU and also using the acceleration by the GPU-based conformation generation and scoring function evaluation approach. The same complexes were also docked with the optimized CPU-based

**Table 1.** Results Obtained for the Sequential CPU Implementation Using Scoring Function PLANTS<sub>chemplp</sub> and Settings Derived from the Search Parameter Optimization for the Parallel Algorithm<sup>a</sup>

| setting                  | success rate (%) up to rank |        |        |          | evaluations<br>( $\times 10^6$ ) |
|--------------------------|-----------------------------|--------|--------|----------|----------------------------------|
|                          | 1                           | 3      | 10     | time (s) |                                  |
| CPU                      |                             |        |        |          |                                  |
| speed1                   | 82 (1)                      | 90 (1) | 94 (1) | 40.3     | 2.75                             |
| speed2                   | 81 (2)                      | 89 (1) | 92 (1) | 19.5     | 1.34                             |
| speed4                   | 77 (2)                      | 85 (2) | 89 (1) | 8.5      | 0.59                             |
| CPU (Parallel Algorithm) |                             |        |        |          |                                  |
| chemplp_gpu1             | 81 (2)                      | 89 (2) | 92 (1) | 62.8     | 3.81                             |
| chemplp_gpu2             | 81 (1)                      | 89 (2) | 92 (1) | 47.8     | 2.90                             |
| chemplp_gpu3             | 80 (2)                      | 88 (2) | 91 (1) | 39.0     | 2.31                             |
| chemplp_gpu4             | 78 (2)                      | 86 (2) | 90 (2) | 23.3     | 1.38                             |
| GPU                      |                             |        |        |          |                                  |
| chemplp_gpu1             | 82 (2)                      | 90 (1) | 93 (1) | 10.0     | 3.84                             |
| chemplp_gpu2             | 81 (2)                      | 89 (1) | 92 (2) | 7.5      | 2.91                             |
| chemplp_gpu3             | 80 (2)                      | 88 (2) | 92 (1) | 5.4      | 2.31                             |
| chemplp_gpu4             | 78 (3)                      | 86 (2) | 90 (2) | 3.6      | 1.38                             |

<sup>a</sup> All results are averaged over 25 independent pose prediction experiments carried out for 129 protein–ligand complexes of the CCDC/Astex clean list<sup>nc</sup> containing no metal ions and with ligands having between 0 and 10 rotatable bonds. The average docking time per ligand was measured on a single core of a Pentium 4, 3.0 GHz processor for the purely CPU-based sequential approach (CPU) and the parallel algorithm running on the CPU [CPU (parallel algorithm)]. The same processor in combination with a Nvidia GeForce 8800 GTX GPU was used for the GPU-accelerated approach (GPU). Standard deviations for the success rates are given in parentheses.

sequential PLANTS algorithm considering the previously optimized search parameter settings speed1, speed2, and speed4.<sup>4</sup>

Table 1 presents results for scoring function PLANTS<sub>chemplp</sub> and the three PLANTS approaches. For each setting, the average success rate for solutions up to rank 1, rank 3, and rank 10 (the ranks correspond to the structures returned by the clustering algorithm mentioned above), the average search time per ligand and the average number of scoring function evaluations performed are reported.

In general, similar average success rates as for the sequential version can be obtained when using the parallel algorithm. However, the parallel algorithm needs on average a much higher number of scoring function evaluations to reach these success rates. For the high-reliability search settings speed1/chemplp\_gpu1, the parallel version running on the CPU needs on average approximately 50% more time than the optimized CPU-based sequential algorithm (around 60 s versus 40 s per ligand). The GPU-accelerated version carries out the same number of scoring function evaluations only using a quarter of the run time (around 10 s per ligand). Thus, the average speedup of the GPU-accelerated approach is around 4 and 6 when compared to the optimized CPU-based sequential approach and the parallel version running on the CPU, respectively. An in-depth analysis of the individual speedup factors observed for the test set instances when using scoring function PLANTS<sub>chemplp</sub> is presented in Figure 8a,b, which gives the dependence of the speedup

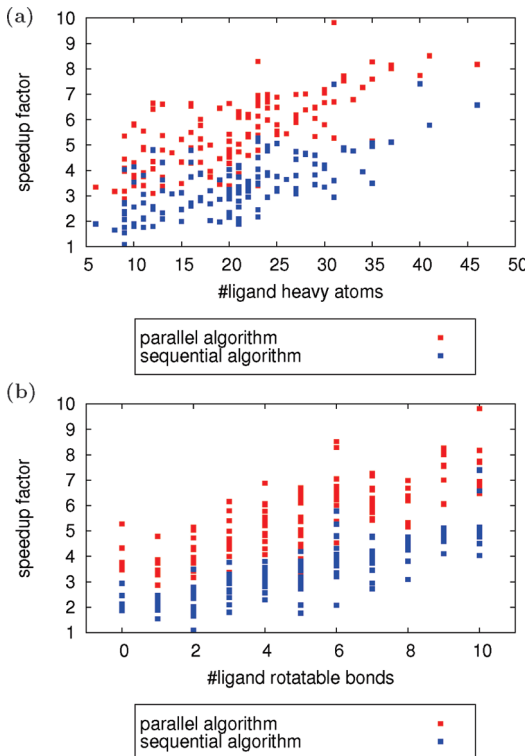


**Figure 8.** Individual speedup factors obtained for the 129 protein–ligand complexes docked using scoring function PLANTS<sub>chemplp</sub> with the high reliability settings. The speedup factors are calculated for the GPU-accelerated version compared with the CPU-based sequential version and the parallel algorithm running on the CPU. The speedup factors are reported as a function of the number of (a) ligand heavy atoms and (b) ligand rotatable bonds.

**Table 2.** Comparison of Sampling Times When Running the Fitness Landscape Analysis Using Just the CPU<sup>a</sup> and Using the GPU-Accelerated Approach<sup>b</sup>

| PDB code | run time (min) |        |         |  |
|----------|----------------|--------|---------|--|
|          | CPU            | GPU    | speedup | evaluations <sup>c</sup> ( $\times 10^6$ ) |
| 1acb     | 3484.42        | 67.75  | 51      | 2.05                                       |
| 1ppf     | 3789.07        | 75.94  | 50      | 2.63                                       |
| 2cpk     | 1381.69        | 36.08  | 38      | 2.63                                       |
| 3hfm     | 23121.83       | 381.55 | 60      | 5.62                                       |

<sup>a</sup> Single core of a Pentium 4, 3.0 GHz processor. <sup>b</sup> Same processor in combination with a Nvidia GeForce 8800 GTX GPU. <sup>c</sup> Number of PLANTS<sub>plp</sub> scoring function evaluations.

factors obtained on the number of ligand heavy atoms and ligand rotatable bonds, respectively.

A very encouraging result is that, when considering the sequential algorithm, speedup factors of over 7 (up to 10 for the parallel algorithm) can be observed for the largest ligands in the test set. In general, the speedup factor strongly depends on the number of rotatable ligand bonds (correlation coefficient  $R^2 = 0.60$ , data from the parallel version used). This can be explained by the fact that the number of clash pairs that need to be checked for the ligand scales with the number of rotatable bonds, which in turn drastically increases the arithmetic intensity. The dependence

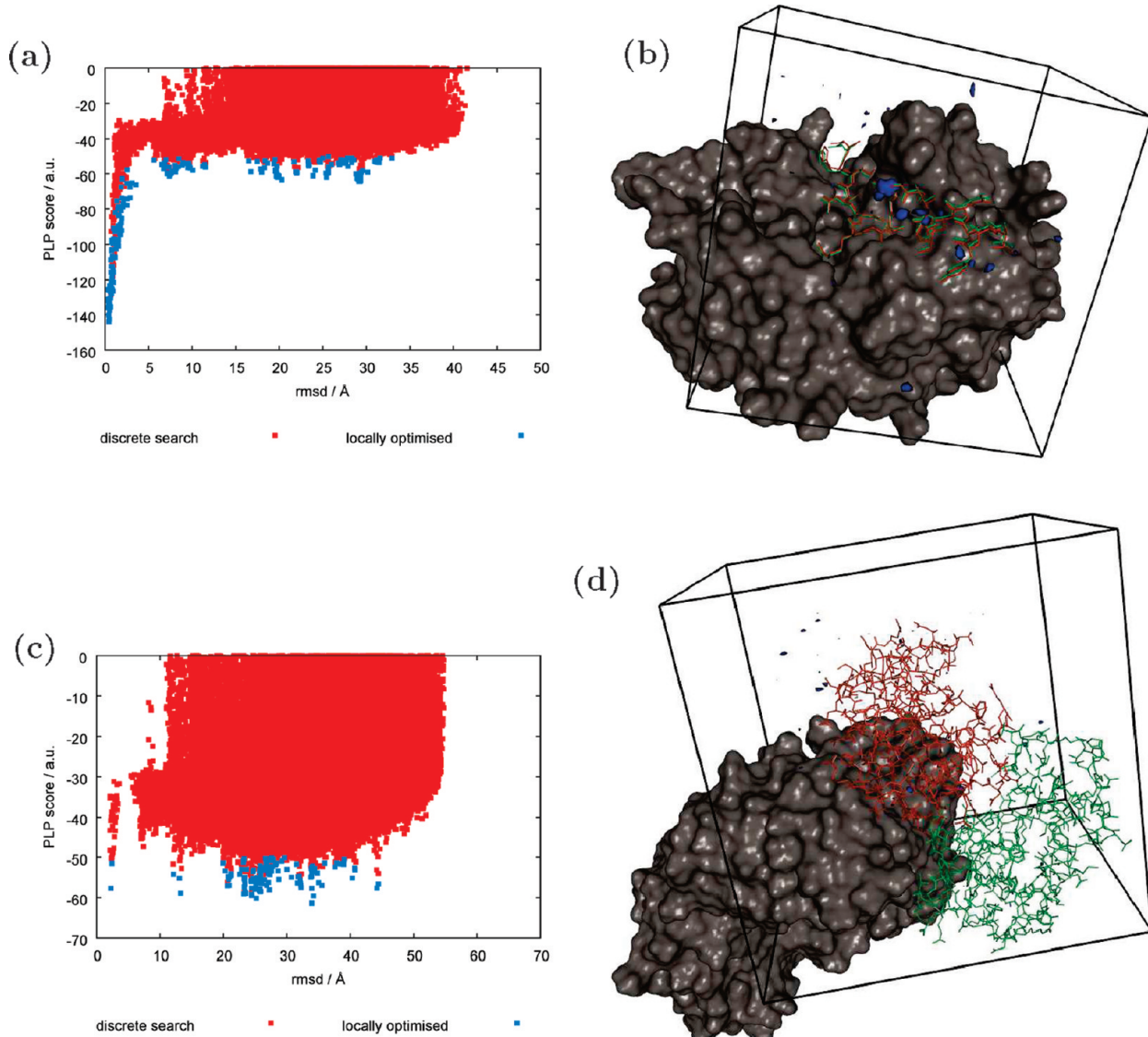


**Figure 9.** Fitness landscapes of two protein–protein complexes (rigid-body docking). Plots (a) and (c) report the rmsd of the docked conformation to the crystal structure ( $x$  axis) versus the scoring function value ( $y$  axis). Data points colored in red resulted from the discrete grid-based search, while blue ones resulted from a local minimization of conformations with a score lower than  $-50.0$  au. Data points of conformations with highly repulsive interactions (positive scoring function values) were omitted. (b,d) Grids (black boxes) used for the systematic sampling along with the experimentally observed mobile protein conformation (red) and the best one resulting from the local minimization (green). Additionally isosurfaces for grid positions which resulted in a score lower than  $-50.0$  au are shown in blue. The fitness landscapes correspond to PDB codes (a,b) 2cpk and (c,d) 3hfm.

on the number of ligand heavy atoms is comparable. A crude correlation ( $R^2 = 0.53$ , data from the parallel version used) between the speedup factor and the number of ligand heavy atoms is obtained.

The observation that the parallel version needs many more scoring function evaluations to achieve an optimization performance similar to that of the sequential version becomes even more apparent at faster search settings. A trend can be seen when calculating the ratio of the number of scoring function evaluations carried out for the GPU and CPU versions for settings that reach similar average success rates. According to Table 1, this ratio increases with decreasing computation times from 1.39 to 2.17 and 2.34 when comparing settings chemplp\_gpu1/speed1, chemplp\_gpu2/speed2, and chemplp\_gpu4/speed4, respectively. In general, the need for a higher number of scoring function evaluations can be attributed to a less efficient optimization

performance. One obvious reason is the smaller number of ACO iterations carried out in the parallel version. In most cases, no search diversification is executed, which usually has a highly beneficial effect on optimization performance. Additionally, the refinement local search step is missing in the parallel version of PLANTS. The current implementation using multiple ant colonies cannot fully compensate for these differences. Similar trends were observed for scoring function PLANTS<sub>PLP</sub> and the results are reported in Table S6 in the Supporting Information.

**Fitness Landscape Analysis.** The fitness landscape analysis using the systematic grid-based sampling methodology described above was performed for four of 18 protein–protein complexes (PDB codes 1acb, 1ppf, 2cpk and 3hfm), covering the smallest and largest problem instances. For all uniform grids used in the systematic search, a grid resolution of  $0.5 \text{ \AA}$  was used, resulting in

approximately 0.5 and 1.4 million grid points for the protein–protein complexes of PDB codes 1acb and 3hfm, respectively. The sampling times when using the CPU- and GPU-based versions, the speedup factors, and the numbers of scoring function evaluations performed are reported in Table 2. As expected, the quite striking speedup factors between 38 and 60 approximately follow those observed earlier for the assessment of the scoring function evaluation performance in Figure 6. These times exclude the time needed for the rigid-body local minimization step applied to the best structures identified by the systematic search (all structures with a score lower than  $-50.0\text{ au}$ ). For the test cases studied, only between 119 (PDB code 1acb) and 236 (PDB code 2cpk) structures were minimized, which resulted in a negligible time overhead of less than 1 min per PDB code.

The fitness landscapes obtained (i.e., the rmsd values of the conformations sampled in the systematic search and those resulting from the local minimization plotted versus the PLANTS<sub>plp</sub> scoring function value of the respective conformation) can be found in Figure 9a (PDB code 2cpk) and 9c (PDB code 3hfm). For PDB code 2cpk, the best-scoring conformation resulting from the local minimization step (score  $-143.94\text{ au}$ ) shows a perfect match with the experimentally observed one (heavy-atom rmsd of  $0.48\text{ \AA}$ ). When looking at the distribution of local optima, in terms of the scoring function value, the global best conformation can be clearly distinguished from the rest. The experimentally observed conformation (colored in red) and the docked conformation (colored in green) are shown in Figure 9b, along with the fixed protein structure and the box showing the boundaries of the uniform grid used for the systematic sampling. Additionally, blue isosurfaces mark regions in the binding site where conformations with a score lower than  $-50.0\text{ au}$  were sampled (used as the starting structures for the local minimization). In contrast, for PDB code 3hfm, a highly frustrated fitness landscape is observed (see Figure 9c). Many of the local optima resulting from the local minimization, although structurally dissimilar, are in a similar score range, and the best conformation found (score of  $-61.53\text{ au}$ ) represents a docking failure (rmsd of  $33.96\text{ \AA}$ , see Figure 9d). Although the global optimum does not agree with the experimental structure, one conformation similar to the experimentally observed one was still sampled and had an heavy-atom rmsd of  $2.26\text{ \AA}$  (score  $-57.75\text{ au}$ ).

The results obtained from this kind of analysis might be helpful in explaining the sampling performance of stochastic global optimization algorithms or the design of scoring functions for protein–protein docking.

## CONCLUSIONS

In this work, we introduced a novel GPU-accelerated conformation generation and scoring function evaluation approach for two empirical scoring functions. The performance of the methodology was assessed for protein–ligand and protein–protein complexes. In the case of protein–ligand systems, the ligand was treated as flexible, and donor groups in the protein binding site were allowed to rotate for scoring function PLANTS<sub>chemplp</sub>. For the largest ligands in the test set and 4000 concurrently scored ligand structures, striking speedup factors of up to over 16 could be observed when comparing the GPU-accelerated approach to the optimized CPU-based implementation. The full potential of the GPU-based scoring function evaluation could be exploited for the protein–protein complexes where the mobile protein was kept rigid. For these experiments, even speedup factors of over 50 were obtained for the largest test set instances.

To demonstrate the practical relevance of the proposed approach, we also presented a parallel version of the PLANTS algorithm and a systematic grid-based sampling approach, both integrating the GPU-accelerated conformation generation and the scoring function evaluation step. In the area of flexible protein–ligand docking, a compromise had to be found between the number of complex conformations scored in parallel and the optimization performance of the docking algorithm. We identified several well-performing settings, which achieved a state-of-the-art pose prediction performance of around 80% over the whole test set of 129 protein–ligand complexes containing small to medium-sized problem instances. The GPU-accelerated version was compared to the optimized CPU-based sequential version<sup>4</sup> and the parallel version running on the CPU. For the high-reliability search settings, average speedup factors of 4 and 6, respectively, were obtained. The speedup factors ranged from nearly no speedup for very small and rigid ligands to factors of 10 (7 for the sequential version) for the largest ligands in the data set. Much larger speedup factors of up to 60 were obtained for the fitness landscape analysis carried out in the context of rigid protein–protein docking. The large difference in the speedup factors observed for flexible protein–ligand and rigid protein–protein docking can be mainly attributed to the size of the problem instances investigated in the two cases. Whereas the mobile protein for protein–protein docking usually consists of several hundred atoms so that high speedup factors can be gained, the ligands in the protein–ligand docking problem usually consist of at most several tens of atoms.

The speedup factors observed especially for the small ligands are limited by several factors. First, only the ligand and protein conformation generation and scoring function evaluation are carried out on the GPU whereas the optimization algorithm is run on the CPU. This algorithmic decomposition implies time-consuming data transfers from the CPU to the GPU and especially vice versa. Ideally, both optimization algorithms (i.e., the ant colony optimization algorithm and the Nelder–Mead simplex algorithm) should also run on the GPU in order to avoid most of the data transfers. However, a GPU-implementation of both optimization approaches is a nontrivial task, as an efficient algorithmic decomposition fitting the GPU architecture needs to be designed. The second bottleneck is the optimization performance of the proposed parallel ACO algorithm, which requires a higher number of scoring function evaluations compared to the CPU-based sequential version in order to reach a similar average success rate. Finally, the current approach explicitly uses the graphics pipeline, which results in some limitations arising from the restricted programming model. Recently introduced special libraries such as Nvidia's compute unified device architecture (CUDA), AMD's Stream technology, and OpenCL allow for explicit general-purpose computation on the GPU and offer a much more flexible programming model. Thus, these libraries will be investigated for the proposed approach in the future. The GPU-accelerated scoring function evaluation approach can also be integrated into other existing docking approaches, profiting from performing concurrent scoring function evaluations. The additional computational power offered by a GPU could also be used to either consider additional degrees of freedom for the docking problem, such as explicit or implicit water molecules, receptor flexibility, and so on, or to screen even larger databases in the context of virtual screening applications.

## ■ ASSOCIATED CONTENT

**S Supporting Information.** Description of additional textures used in the GPU-based approach, PDB codes for the protein–protein docking data set, assessment of CPU- and GPU-based scoring function evaluation accuracy, speedup factors obtained for scoring function PLANTS<sub>chemplp</sub> and optimized search parameter settings and docking results for scoring function PLANTS<sub>plp</sub>. This information is available free of charge via the Internet at <http://pubs.acs.org/>.

## ■ AUTHOR INFORMATION

### Corresponding Author

\*Phone: +44 1223 763923 (O.K.), +49 7531 882015 (T.E.E.). Fax: +44 1223 336033 (O.K.), +49 7531 883587 (T.E.E.). E-mail: korb@ccdc.cam.ac.uk (O.K.), thomas.exner@uni-konstanz.de (T.E.E.).

## ■ ACKNOWLEDGMENT

The authors thank Prof. Dr. Jürgen Brickmann, MolCad GmbH, for supplying the computer hardware used to carry out the research. O.K. acknowledges support from the Landesgradiertenförderung Baden-Württemberg, the Cambridge Crystallographic Data Centre, and the Postdoc-Programme of the German Academic Exchange Service (DAAD). T.S. acknowledges support from the Belgian F.R.S.-FNRS, for which he is a research associate.

## ■ REFERENCES

- (1) Moitessier, N.; Englebienne, P.; Lee, D.; Lawandi, J.; Corbeil, C. R. Towards the development of universal, fast and highly accurate docking/scoring methods: A long way to go. *Br. J. Pharmacol.* **2008**, *153*, S7–S26.
- (2) Korb, O.; Stützle, T.; Exner, T. E. PLANTS: Application of Ant Colony Optimization to Structure-Based Drug Design. In *Ant Colony Optimization and Swarm Intelligence, 5th International Workshop, ANTS 2006*; Dorigo, M., Gambardella, L. M., Birattari, M., Martinoli, A., Poli, R., Stützle, T., Eds.; Springer: Heidelberg, Germany, 2006; Vol. 4150, 247–258.
- (3) Korb, O.; Stützle, T.; Exner, T. E. An Ant Colony Optimization Approach to Flexible Protein–Ligand Docking. *Swarm Intel.* **2007**, *1*, 115–134.
- (4) Korb, O.; Stützle, T.; Exner, T. E. Empirical Scoring Functions for Advanced Protein–Ligand Docking with PLANTS. *J. Chem. Inf. Model.* **2009**, *49*, 84–96.
- (5) Fan, Z.; Qiu, F.; Kaufman, A.; Yoakum-Stover, S. GPU Cluster for High Performance Computing. In *SC’04: Proceedings of the 2004 ACM/IEEE Conference on Supercomputing*; IEEE Computer Society: New York, 2004.
- (6) Owens, J. D.; Luebke, D.; Govindaraju, N.; Harris, M.; Krüger, J.; Lefohn, A. E.; Purcell, T. J. A Survey of General-Purpose Computation on Graphics Hardware. *Comput. Graph. Forum* **2007**, *26*, 80–113.
- (7) NVIDIA CUDA Compute Unified Device Architecture Programming Guide; NVIDIA: Santa Clara, CA, 2007.
- (8) Stone, J. E.; Hardy, D. J.; Ufimtsev, I. S.; Schulten, K. GPU-accelerated molecular modeling coming of age. *J. Mol. Graph. Modell.* **2010**, *116*–125.
- (9) Yasuda, K. Accelerating Density Functional Calculations with Graphics Processing Unit. *J. Chem. Theory Comput.* **2008**, *4*, 1230–1236.
- (10) Ufimtsev, I. S.; Martinez, T. J. Quantum Chemistry on Graphical Processing Units. 2. Direct Self-Consistent-Field Implementation. *J. Chem. Theory Comput.* **2009**, *5*, 1004–1015.
- (11) Ufimtsev, I. S.; Martinez, T. J. Quantum Chemistry on Graphical Processing Units. 3. Analytical Energy Gradients, Geometry Optimization, and First Principles Molecular Dynamics. *J. Chem. Theory Comput.* **2009**, *5*, 2619–2628.
- (12) Vogt, L.; Olivares-Amaya, R.; Kermes, S.; Shao, Y.; Amador-Bedolla, C.; Aspuru-Guzik, A. Accelerating Resolution-of-the-Identity Second-Order Moller–Plesset Quantum Chemistry Calculations with Graphical Processing Units. *J. Phys. Chem. A* **2008**, *112*, 2049–2057.
- (13) Friedrichs, M. S.; Eastman, P.; Vaidyanathan, V.; Houston, M.; Legrand, S.; Beberg, A. L.; Ensign, D. L.; Bruns, C. M.; Pande, V. S. Accelerating molecular dynamic simulation on graphics processing units. *J. Comput. Chem.* **2009**, *30*, 864–872.
- (14) Harvey, M. J.; De Fabritiis, G. An Implementation of the Smooth Particle Mesh Ewald Method on GPU Hardware. *J. Chem. Theory Comput.* **2009**, *5*, 2371–2377.
- (15) Stone, J. E.; Phillips, J. C.; Freddolino, P. L.; Hardy, D. J.; Trabuco, L. G.; Schulten, K. Accelerating molecular modeling applications with graphics processors. *J. Comput. Chem.* **2007**, *28*, 2618–2640.
- (16) Roh, Y.; Lee, J.; Park, S.; Kim, J. A molecular docking system using CUDA. In *Proceedings of the 2009 International Conference on Hybrid Information Technology*; ACM: New York, 2009, 28–33.
- (17) Sukhwani, B.; Herbordt, M. C. GPU acceleration of a production molecular docking code. In *GPGPU-2: Proceedings of 2nd Workshop on General Purpose Processing on Graphics Processing Units*; ACM: New York, 2009, 19–27.
- (18) Nissink, J. W. M.; Murray, C.; Hartshorn, M.; Verdonk, M. L.; Cole, J. C.; Taylor, R. A new test set for validating predictions of protein–ligand interaction. *Proteins* **2002**, *49*, 457–471.
- (19) Gehlhaar, D. K.; Verkhivker, G. M.; Rejto, P. A.; Sherman, C. J.; Fogel, D. B.; Fogel, L. J.; Freer, S. T. Molecular recognition of the inhibitor AG-1243 by HIV-1 protease: Conformationally flexible docking by evolutionary programming. *Chem. Biol.* **1995**, *2*, 317–324.
- (20) Munshi, A., Ed. *The OpenCL Specification*, version 1.1; Khronos Group: Beaverton, OR, 2010; <http://www.khronos.org/registry/cl/specs/opencl-1.1.pdf> (accessed Jan 31, 2010).
- (21) Berman, H.; Westbrook, J.; Feng, Z.; Gilliland, G.; Bhat, T.; Weissig, H.; Shindyalov, I.; Bourne, P. The Protein Data Bank. *Nucl. Acids Res.* **2000**, *28*, 235–242.
- (22) Bullnheimer, B.; Kotsis, G.; Strauss, C. Parallelization Strategies for the Ant System. In *High Performance Algorithms and Software in Nonlinear Optimization*; Leone, R. D., Murli, A., Pardalos, P., Toraldo, G., Eds.; Kluwer Series of Applied Optimization 24; Kluwer Academic Publishers, Dordrecht, The Netherlands, 1998.
- (23) Talbi, E.-G.; Roux, O.; Fonlupt, C.; Robillard, D. Parallel ant colonies for the quadratic assignment problem. *Fut. Gen. Comput. Syst.* **2001**, *17*, 441–449.
- (24) Middendorf, M.; Reischke, F.; Schmeck, H. Multi Colony Ant Algorithms. *J. Heuristics* **2002**, *8*, 305–320.
- (25) Manfrin, M.; Birattari, M.; Stützle, T.; Dorigo, M. Parallel Ant Colony Optimization for the Traveling Salesman Problem. In *Ant Colony Optimization and Swarm Intelligence, 5th International Workshop, ANTS 2006*; Dorigo, M., Gambardella, L. M., Birattari, M., Martinoli, A., Poli, R., Stützle, T., Eds.; Springer: Heidelberg, Germany, 2006; Vol. 4150, 224–234.
- (26) Scheuermann, B.; So, K.; Guntsch, M.; Middendorf, M.; Diessel, O.; ElGindy, H. A.; Schmeck, H. FPGA implementation of population-based ant colony optimization. *Appl. Soft Comput.* **2004**, *4*, 303–322.
- (27) Nelder, J. A.; Mead, R. A simplex method for function minimization. *Comput. J.* **1965**, *7*, 308–313.
- (28) Press, W. H.; Flannery, B. P.; Teukolsky, S. A.; Vetterling, W. T. *Numerical Recipes in C: The Art of Scientific Computing*; Cambridge University Press: New York, 1992.
- (29) Case, D. A.; Cheatham, T. E.; Darden, T.; Gohlke, H.; Luo, R.; Merz, K. M.; Onufriev, A.; Simmerling, C.; Wang, B.; Woods, R. J. The Amber biomolecular simulation programs. *J. Comput. Chem.* **2005**, *26*, 1668–1688.